# CONTROLLED CONTAMINATION OF EPOXY COMPOSITES WITH PDMS AND REMOVAL BY LASER ABLATION

Frank Palmieri[1], Rodolfo Ledesma[2], Daniel Cataldo[1], Yi Lin[3], Christopher Wohl[1], Mool Gupta[2], and John Connell[1]

1. NASA Langley Research Center, Hampton, VA 23681
2. University of Virginia, Charlottesville, VA
3. National Institute of Aerospace, Hampton, VA

## ABSTRACT

Surface preparation is critical to the performance of adhesively bonded composites. During manufacturing, minute quantities of mold release compounds are inevitably deposited on faying surfaces and may compromise bond performance. To ensure safety, mechanical fasteners and other crack arrest features must be installed in the bondlines of primary structures, which negates some advantages of adhesively bonded construction. Laser ablation is an automated, repeatable, and scalable process with high potential for the surface preparation of metals and composites in critical applications such as primary airframe structures. In this study, laser ablation is evaluated on composite surfaces for the removal of polydimethylsiloxane (PDMS), a common mold release material. Composite panels were contaminated uniformly with PDMS film thicknesses as low as 6.0 nm as measured by variable angle spectroscopic ellipsometry. Bond performance was assessed by mechanical testing using a 250 °F cure, epoxy adhesive and compared with pre-bond surface inspection results. Water contact angle, optically stimulated electron emission, and laser induced breakdown spectroscopy were used to characterize contaminated and laser ablated surfaces. The failure mode obtained from double cantilever beam tests correlated well with surface characterization data. The test results indicated that even low levels of PDMS were not completely removed by laser ablation.

## 1. INTRODUCTION

Adhesive bonding has several advantages over mechanical fastening, particularly in the assembly of composite structures, by reducing manufacturing cost and improving airframe performance [1-2]. But to attain FAA certification, redundant load paths (e.g. mechanical fasteners) are required in secondary-bonded, primary structures (SBPS) because no nondestructive methods exist to directly measure the strength of an adhesive bond. A repeatable and effective surface treatment is a key component of an overall manufacturing methodology for the certification of SBPS.[2-4] Complementary metrology techniques are needed for fast, in-line assessment of prepared surfaces to assure repeatable bond performance without destructive testing [5-6].

### 1.1 State-of-the-Art Surface Preparation

Current surface preparation methods rely on mechanical processes to create roughness and reactive surface chemistry. The most common techniques are sanding, grit blasting, and peel-ply. Sanding and grit blasting can be difficult to automate and involve a significant amount of human intervention and judgment, which may be a source of variability. In addition, mechanical abrasion can result in fiber damage and leave behind or even embed debris, which is often cleaned using

solvent [7-8]. A peel ply may also leave behind residual debris or a layer of contamination that must be removed before bonding. For acceptable bond performance, the correct peel ply fabric must be paired with a resin matrix, further complicating its use [9-10].

### 1.2 Laser Surface Preparation

In contrast to mechanical abrasion and peel ply techniques, laser surface treatment offers a controllable, repeatable, and scalable solution to prepare composite surfaces for bonding [11-12]. By monitoring laser power, focus, pulse frequency, and translation speed, the surface properties can be closely controlled [13]. Ablation is the vaporization and ejection of material from a surface due to the absorption of intense radiation. The wavelength, pulse duration, fluence, and scan parameters of the laser can be set to selectively ablate a matrix resin without damaging the carbon fiber. In Fisher et al., it is suggested that maximal epoxy should be removed, while keeping the structure of the load-bearing fibers intact, to enable direct load introduction to the fibers [14-15].

Previous work established a process for laser-treated CFRP surfaces using a frequency tripled (355 nm), nanosecond, Nd:YAG laser at varying average laser power and areal coverage [15-16]. The laser parameters that gave optimal bond performance based on mode I mechanical tests were used in this report to study the removal of contaminates.

### 1.3 Pre-bonding Surface Inspection

The manufacture of predictable secondary bonds may depend on an accurate assessment of prepared surfaces just prior to bonding. The detection of organic contaminates is particularly challenging on composite surfaces, which are primarily composed of carbon. High-vacuum techniques (X-ray photoelectron spectroscopy and ion scattering spectroscopy) can provide quantitative composition information for the uppermost atomic layers of a surface but are not practical for in-line quality assurance. Infrared spectroscopy coupled with chemometrics and water contact angle (WCA) techniques are being developed for the in-line detection surface contaminant concentrations as low as 1 $mg/cm^2$ [6, 17]. However, some common contaminants (e.g. mold release compounds such as polydimethylsiloxane, PDMS) may diminish bond performance at concentrations less than 1 $mg/cm^2$.

Optically stimulated electron emission (OSEE) was developed primarily for inspection of metallic surfaces for grease residue, while laser induced breakdown spectroscopy (LIBS) is a surface analysis technique. Both methods may be effective for in-line inspection of composite surfaces. In OSEE, the electric current emitted from a surface exposed to deep ultra violet (DUV) radiation is highly sensitive to surface contamination. Materials with relatively small work functions (i.e. conductors) emit electrons in DUV while dielectrics are far less likely to emit. The inspection is fast, and can provide a quantitative assessment of surface contamination levels. The work function of emitted electrons is not measured, so no spectral data are available to directly determine the surface chemical composition [18]. In LIBS, radiation from a plasma plume produced during laser ablation is collected and spectroscopically interrogated. The resulting spectrum contains information about surface composition and relative abundance. LIBS systems, including hand-held devices, have been recently commercialized for identifying metals, and similar technology may be applicable to composites surfaces. LIBS could be integrated with the laser surface preparation process to provide real time in-situ monitoring of the surface chemistry and closed-loop control of the ablation process.

### 1.4 Contents of this Report

Surface characterization techniques were investigated to predict bond performance of CFRP substrates contaminated with discrete levels of PDMS in the thickness range of 5 – 1500 nm. PDMS was selected as the contaminant because it is widely used in mold release products that are prevalent in the fabrication of composites, and it is suspected to affect bond performance at relatively low concentrations. Film thicknesses less than 100 nm were characterized via ellipsometry while thicker films were measured by mass change. A double cantilever beam (DCB) test was performed on bonded specimens to compare the failure mode and average fracture toughness ($G_{AVG}$) with water contact angle, OSEE and LIBS results for three discrete levels of PDMS contamination.

## 2. EXPERIMENTATION

### 2.1 Materials

For mechanical testing, carbon fiber reinforced plastic (CFRP) panels (30.5 cm × 30.5 cm (12 in × 12 in) were prepared from 10 plies of Torayca P2302-19 prepreg tape (T800H/3900-2 carbon fiber/toughened epoxy resin system) and cured in an autoclave at 177 °C (350 °F) and 690 kPa (100 psi). Release from the caul plate was accomplished using Airtech A4000 release film (fluorinated ethylene propylene, FEP). For OSEE and LIBS experiments, 8-ply CFRP panels (30.5 cm × 30.5 cm, 12 in × 12 in) were prepared in the same fashion and cut into 3.8 cm × 3.8 cm coupons. The adhesive used for bonding mechanical test specimens was Hysol EA9696 from Henkel Corporation (cured in an autoclave at 121 °C or 250 °F) and 0.34- 0.68 MPa (50-100 psi). Silicon wafers (10.2 cm diameter, [100] crystal orientation), used for contaminant metrology, were obtained from Silicon Materials Inc. Aluminum coupons (10.2 cm × 10.2 cm × 0.02 cm), used for high contamination metrology, were obtained from McMaster Carr. The contaminant was PDMS, 980 cP obtained from Brookfield Engineering, and had a number average molecular weight ($M_n$) of 35,400 ± 4,100 g/mol and a polydispersity of 1.8 ± 0.18, measured in toluene with an Agilent GPC 220 high temperature gel permeation chromatograph by the triple detection method. Hexanes and isopropanol were obtained from Fisher Scientific.

### 2.2 Contamination Method

CFRP panels were wiped with isopropanol before coating with a solution of PDMS in hexanes. Three stock solutions with concentrations of 0.05 wt%, 0.5 wt% and 6 wt% were spray coated to produce low, medium, and high levels of contamination, respectively. Preliminary experiments established a correlation between the concentration of PDMS ($P$) in wt% and film thickness ($t$) in nanometers given by the proportion

$$t = 177.6\,P$$

An airbrush set (Badger Model 350) and an air compressor (AirBrush-Depot Model TC-20) set to 0.27 MPa (40 psi) were used to apply coatings at room temperature. The spray gun was cleaned before coating by spraying hexanes and rinsing the siphon tube with hexanes. The level of solution in the reservoir significantly impacted the mass flow rate from the airbrush, so the solution was continuously replenished while coating. Each CFRP panel was mounted vertically with either a witness silicon wafer or aluminum coupon and a smaller CFRP coupon for OSEE and LIBS testing. Two mechanical jacks were used to adjust the height of the spray gun by 1.82 cm (0.72 in)

for each spray pass. A constant distance, 8.60 cm (3.39 in), was maintained between the airbrush and the substrates. All coated substrates were heated at 120 °C (248 °F) in an air oven for one hour to fully vaporize residual hexanes.

Table 1: Experiment matrix for contaminated specimen preparation.

| Contamination Level | Surface Treatment | Concentration of PDMS in Hexanes (%) | Contamination Thickness (nm) | Areal Density of Contamination (μg/cm$^2$) |
|---|---|---|---|---|
| Control | Laser | Uncoated | 0.0 | 0.0 |
| Low | Laser | 0.05 | 8.0 ± 1.6 | 0.8 |
| Medium | Laser | 0.5 | 59.7 ± 14.1 | 5.8 |
| High | Laser | 6 | 1310.0 ± 51.0 | 126.5 |
| Low | Untreated | 0.05 | 10.8 ± 27.4 | 1.0 |

### 2.3 Contamination Metrology

Levels of contamination were characterized by either spectroscopic ellipsometry performed on witness silicon wafer, or via mass change of witness aluminum coupons. The high contamination level could not be measured by ellipsometry due to film thickness variation while the mass changes for low and medium levels of contamination were too small to be detected by an analytical balance.

#### 2.3.1 Ellipsometry

Spectroscopic ellipsometry is a well-established technique to characterize the optical properties and thickness of submicron, uniform, transparent films on optically flat substrates, such as silicon wafers, nondestructively [19]. Variable angle spectroscopic ellipsometry (VASE) was performed on silicon wafers with low and medium contamination levels using a J.A. Woollam Co. VB-400 VASE and HS-190 monochromator. Data were collected for wavelengths between 300 nm and 900 nm in increments of 10 nm at three angles of incidence: 65°, 70°, and 75°. Scan settings were set to 10 revolutions per measurement, and the sample was treated as isotropic. For each wafer, five locations spaced by 0.36 cm (0.14 in) were scanned to collect data equally from the entire path width of the contamination spray plume. Empirical models based on refractive index (*n*) and extinction coefficient (*k*) were used to predict unknown film thicknesses. The model used for the silicon substrate was ("Si_Jaw") and that for the silicon dioxide layer was ("SiO2_Palik") [20-21]. A native oxide thickness of 1.8 nm was measured from an uncontaminated wafer, and *n* and *k* were optimized. A PDMS model layer ("PDMS.g") was added above the $SiO_2$ layer to model the contaminated silicon wafers and determine the PDMS layer thickness.

#### 2.3.2 Mass Change

Prior to spraying, aluminum coupons were weighed on an analytical balance with 0.01 mg resolution. The mass of the coupon was measured again after spraying and oven drying. The film thickness was calculated from the mass increase, coupon surface area and density of PDMS (0.965 g/ml).

## 2.4 Laser Processing and Surface Morphology Evaluation

Laser ablation was performed on all panels (with the exception of test 7) with a PhotoMachining, Inc. system with a Coherent®, Avia®, frequency tripled, Nd:YAG laser (7 W nominal pulsed output at 355 nm and 10 ns pulse duration). A galvanometer was used to scan the laser spot across the stationary composite panels at a speed of 25.4 cm/s (10 in/s) during ablation. A thermopile sensor (model 3A-SH) and Nova II power meter from Ophir Spirocon LLC were used to monitor the average laser power. Laser ablation produced parallel lines in the fiber direction at an average power of 800 mW, pulse frequency of 80 kHz, and a line pitch of 23 μm (0.0009 in), which gave 105% areal coverage (i.e. a small overlap between two adjacent laser passes), a scan speed of 25.4 cm/s (10 in/s) and an average fluence of 15.1 J/cm$^2$. Uncontaminated panels were thoroughly wiped with lint free, isopropanol wetted tissue prior to laser treatment. Surface morphology of laser ablated CFRP coated with Pd-Au was evaluated using a JEOL JSM 5600F scanning electron microscope (SEM) operated at an accelerating voltage of 10 – 15 kV.

## 2.5 Bonding and DCB Testing

Within 48 h of ablation, pairs of panels were bonded in an autoclave at 121 °C (250 °F) and 0.34 - 0.68 MPa (50-100 psi). A 7.62 cm (3 in) long, 12.5 μm thick film of FEP was included in the layup to create a precrack. Using a modification of ASTM D5528-13, samples were machined with a water jet into 5, 2.5 cm x 24.1 cm (1 in in x 9.5 in) specimens with notched ends for mounting directly on a clevis grip without need for bonding block, hinges or drilling [22]. The modified specimen geometry can be seen in Figure 1.

Prior to mechanical testing, one side of the test specimen was painted silver to improve visibility of the crack. The clevis grips were installed by opening the specimen end approximately 5 mm, and the initial crack location was marked by visual inspection with a 10× magnifying glass. An Instron® 5848 Microtester and 500 N load cell were used to record the applied load and displacement at a crosshead speed of 5 mm/min to an extension of 90 mm. A Nikon D800e camera with a 105 mm macro lens controlled with Nikon Camera Control Pro 2 software captured the crack profile once every 5 seconds up to 5 mm of crack growth and once every 15 seconds for the remainder of the test. Upon test completion, the final crack position was marked on the specimen.

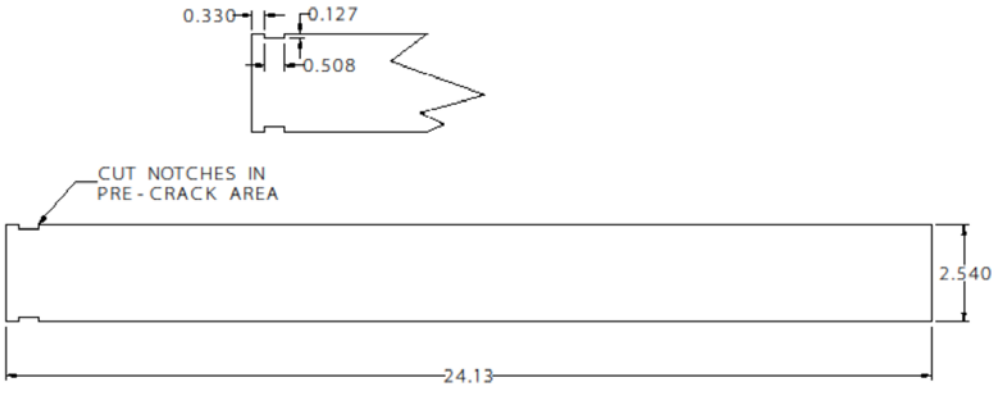


Figure 1: DCB Specimen geometry. Notches are for securing specimen to clevis grip. Measurements are in centimeters.

## 2.6 Failure Mode and Fracture Toughness Analysis

Failed surfaces were scanned using an Epson V600 scanner at 24 bit color and 600 dpi resolution. The failure mode was digitally analyzed by color threshold analysis using the ImageJ software, visual inspection, and guidance from ASTM D5573 [23]. Outlier values were removed for each failure mode category. The resulting data were averaged to obtain failure mode data for each test.

Crack length, load, and displacement data were used to calculate the average fracture toughness, $G_{AVG}$, using modified beam theory. The load vs. extension data were offset to correct for preload on the specimen caused by the modified specimen gripping technique. The $G_{AVG}$ values were calculated for steady crack growth, which occurred primarily by cohesive failure. All crack extension data occurring prior to the maximum load point were discarded for uniform analysis. Remaining values were assigned a weighted average based upon the percentage of crack growth they contributed, and summed to obtain $G_{AVG}$ values for each specimen. $G_{AVG}$ outlier values were removed for each specimen within each test.

## 2.7 Contact Angle Measurement

Water contact angles (WCA) were measured using a Surface Analyst$^{TM}$ device from Brighton Technologies Group. For all samples, WCA was measured after contamination (prior to laser ablation), immediately following laser ablation, and again prior to bonding. For the sample with no laser treatment, contact angles were measured after contamination and prior to bonding. The post-ablation measurements were performed on identically treated areas offset from the mechanical specimen region of the panel. Nine WCA drops were measured on each panel for each test. The presented data are the average values from two panels.

## 2.8 Optically Stimulated Electron Emission

The function and design of the OSEE instrument was described by Perey [18]. Interaction with 185 nm radiation from a mercury vapor lamp, a broadband source, produced 95% of the OSEE response from the substrate. The test area (2.54 cm in diameter) was purged with argon, and the distance between the collector and the test surface was approximately 5.2 mm. OSEE measurements were conducted three times on each sample after contamination and again after laser ablation. The highly contaminated specimen was not measured before ablation to avoid contamination of the tool. The reported threshold voltage ($V_{th}$) was measured from a stable region of the emission trace approximately 150 ms after the start of the experiment. A peak voltage ($V_p$) was also observed after longer exposure times but was not reported.

## 2.9 Laser Induced Breakdown Spectroscopy

To accommodate the weak plasma produced by μJoule (μJ) laser pulses, a sufficiently long gate width was set to collect the laser-induced plasma emission from multiple, consecutive pulses. The number of pulses was determined empirically and yielded a sufficient signal-to-noise ratio. Multiple spectra were collected during each multi-pulse experiment. In the μJoule LIBS (μLIBS) process, the line emission was much greater than the continuum emission; therefore, a wide gate, which encompassed both continuum and line emission events, was permissible.

The μLIBS system consists of a Schmidt-Czerny-Turner spectrograph coupled with an emICCD detector. The center wavelength was set to 247 nm to observe the characteristic carbon line

emission at 247.8 nm. The upper-bound of the spectral range was 295 nm, sufficient for detection of silicon line emissions. The collimating lens was aligned at 45$^{o}$ with respect to the sample surface using a XYZ stage to maximize light collection. The laser parameters for µLIBS analysis were 40 kHz pulse frequency, 62.5 µJ pulse energy, and 50 pulses in a fixed location. The apparent spot size was approximately 25 µm for an instantaneous fluence of 13 J/cm$^2$. µLIBS was performed on two substrates: 1) a pristine CFRP surface and 2) a CFRP surface that was contaminated and laser ablated.

# 3. RESULTS & DISCUSSION

## 3.1 Surface Morphology

SEM micrographs of laser ablated composite specimens are shown in figure 2. The ablation process selectively removed surface resin from the composite without ablating the carbon fiber. The ablation process deposited some debris, primarily visible at the edge of the ablation field.

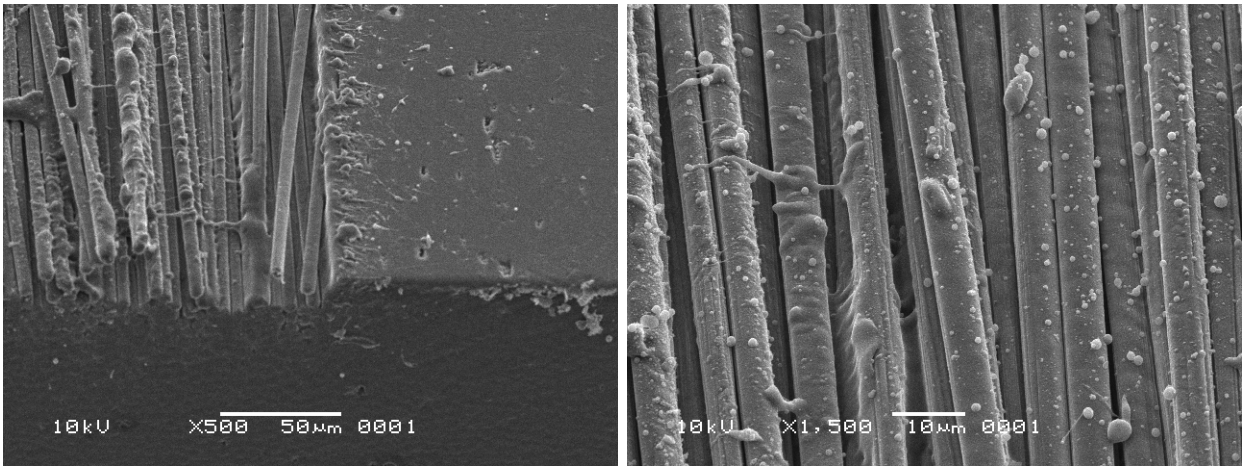


Figure 2: (left) The edge of the ablation field shows ablated and unablated surfaces side by side. (right) A higher magnification image of carbon fibers exposed after ablation.

## 3.2 Pre-bond Surface Inspection

### 3.2.1 Water Contact Angle

WCA data are summarized in figure 3 for all contamination thicknesses and process steps. Except for the high level of contamination, the specimens exhibited the highest WCA imediately after applying the PDMS contaminant. The post contamination WCA correlated directly with contamination thickness but remained significantly lower than the intrinsic WCA on a pure PDMS substrate (110°) [24]. For post-ablation and prebonding, specimens with no, low and medium PDMS levels had statistically equivalent values based on a t test with a 90% confidence level. The roughness of laser treated surfaces may have increased the variation in the WCA data limiting the detection of minute, residual contamination. For the high level of contamination, WCA was not reduced by ablation and after about 48 h, showed an increased WCA, which may be attributed to increased surface roughness and diffusive burial of polar groups into the surface [25].

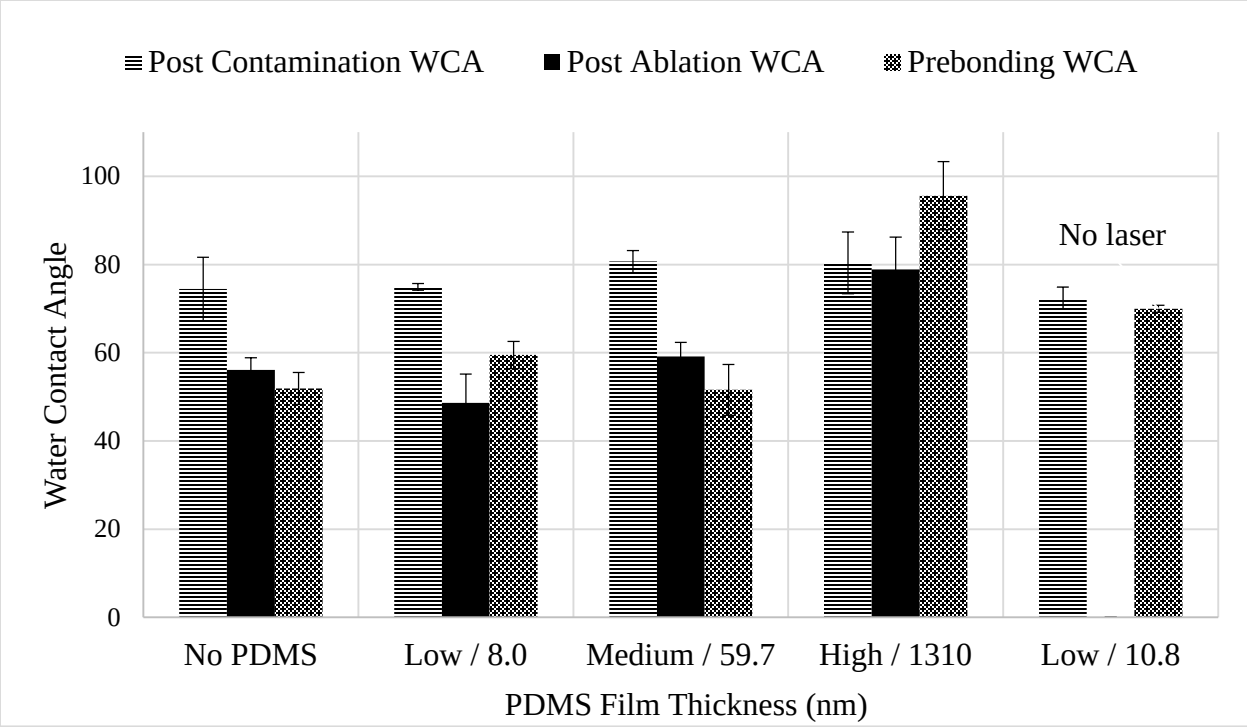


Figure 3: Water contact angle data. Post contamination value for the "No PDMS" samples was measured on the as-received surface. Error bars are one standard deviation.

### 3.2.2 Optically Stimulated Electron Emission

Figure 4 summarizes OSEE results for different surface conditions. The OSEE signal, which measures the emission current from a substrate exposed to DUV radiation, decreased with increasing PDMS contamination thickness and increased dramatically after ablation indicating a change in surface composition. After ablation, $V_{th}$ for contaminated surfaces did not achieve the same value observed for the ablated, uncontaminated surface, which may indicate the presence of residual PDMS. PDMS absorbs strongly at 185 nm, but does not readily emit electrons, therefore, contamination layer thickness correlated directly with $V_{th}$ [26]. The composite matrix resin behaves similarly and reduces $V_{th}$ by covering carbon fibers, which more readily undergo photoemission of electrons. Laser ablation may remove both PDMS and matrix resin simultaneously, which exposed carbon fibers and dramatically increases $V_{th}$.

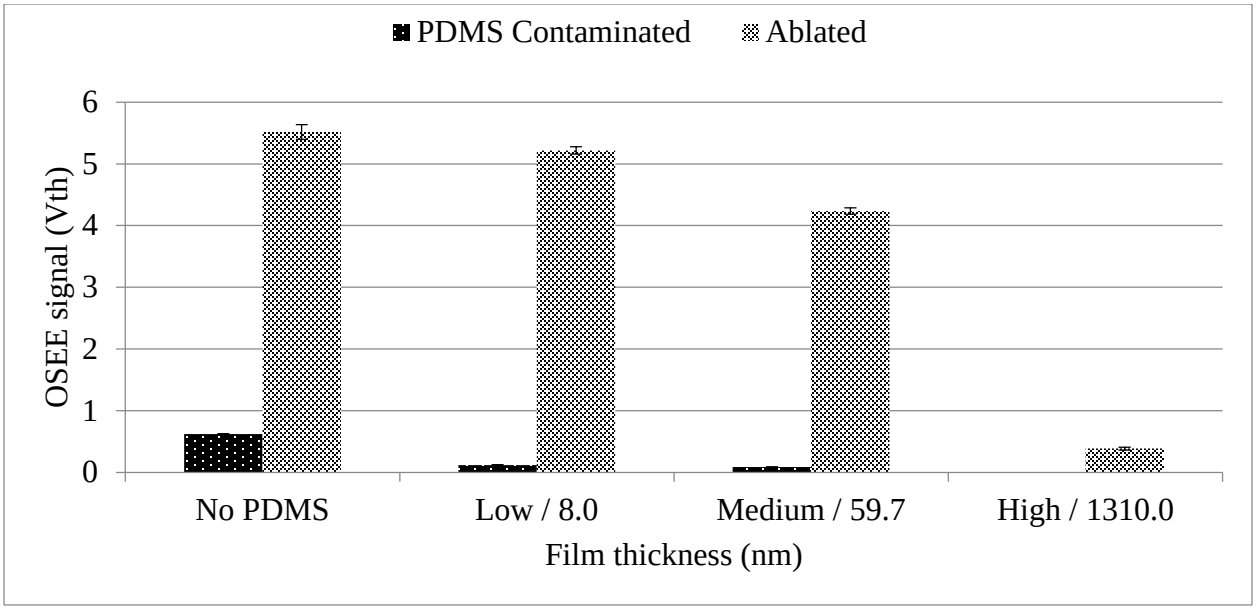


Figure 4. OSEE signal for different film thickness of PDMS on CFRP samples.

### 3.2.3 Laser Induced Breakdown Spectroscopy

Figure 5 shows a µLIBS spectrum for a control CFRP sample with no PDMS coating nor laser ablation treatment. The neutral carbon emission line (C I) was observed at 247.8 nm as well as other less prominent carbon ion species (C II and C III) from the decomposition of the carbon based substrate.

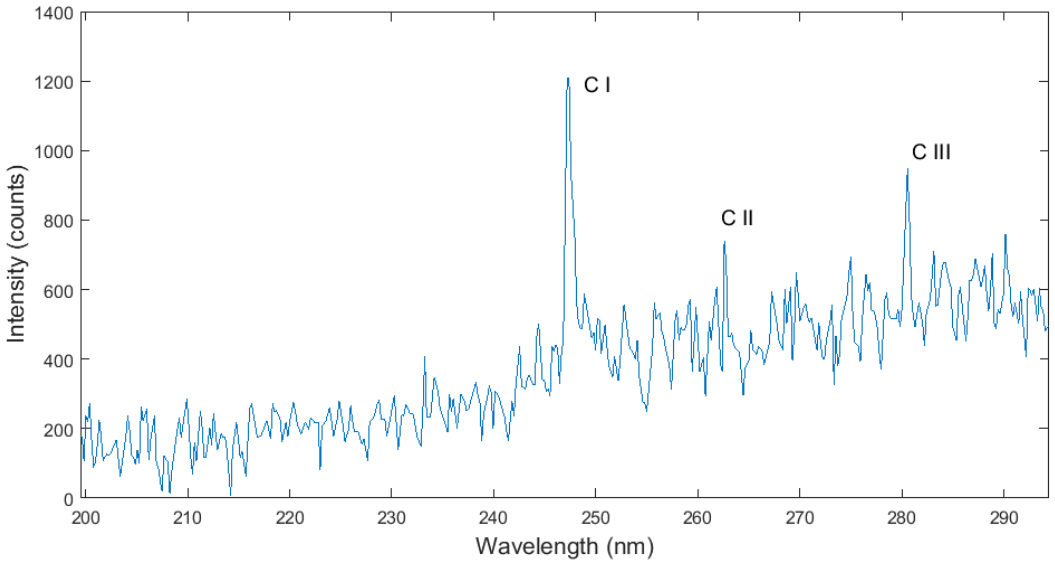


Figure 5. A LIBS spectrum from a 50-pulse experiment on a control CFRP coupon without PDMS or laser treatment.

Figure 6 is a spectrum from a CFRP coupon that was contaminated with a high level of PDMS and then laser ablated. In addition to the C I emission line, Si I (263.1 nm and 288.1 nm) and Si III

(277.2 nm) emissions indicated residues of PDMS not completely removed by laser ablation [27]. The same sample was also inspected by energy dispersive spectroscopy (data not presented) and a silicon signal was detected. This result agreed with the low $V_{th}$ value (figure 4) for the highly contaminated coupon.

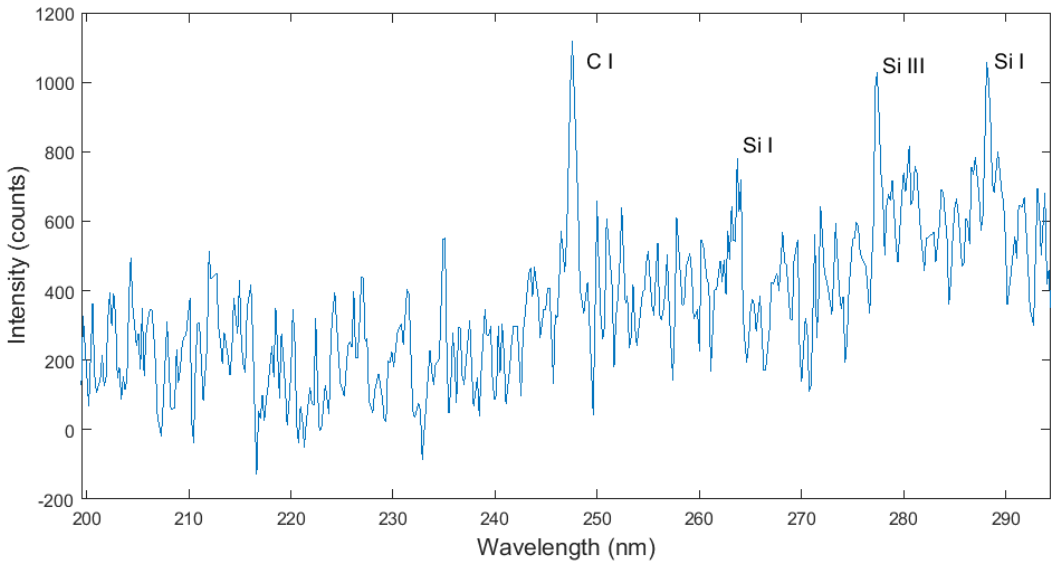


Figure 6. A LIBS spectrum of a CFRP coupon that received the high level of contamination and laser treatment.

### 3.3 Failure Modes

The failure mode data from DCB testing are presented in Figure 7. Predominantly cohesive failure was observed for the uncontaminated, laser ablated baseline sample. With increasing PDMS contamination level, the proportion of cohesive failure diminished dramatically while adhesive failure became the dominant mode indicating poor interfacial adhesion. Good correlation (R = 0.59) between PDMS thickness and percent adhesive failure indicated that increasing contamination level diminishes bond performance. The low contamination level, unablated sample exhibited 100% adhesive failure; therefore, the reduction of adhesive failure in the contaminated samples was attributed to the laser treatment.

The predominance of adhesive failure for PDMS contaminated samples, indicated PDMS residues remained after ablation which might be explained by two distinct mechanisms. First, the laser radiation at 355 nm is poorly absorbed by PDMS and could have prevented the direct decomposition and vaporization of the PDMS layer from the composite surface [28]. The underlying epoxy matrix absorbs strongly at 355 nm, and underwent an explosive decomposition upon laser ablation, which ejected particles from the surface. Particles containing PDMS that were too large to be volatilized or carried away by the atmosphere might have been redeposited onto the CFRP surface. Second, polar groups, such as silanols present in partially decomposed PDMS residues might have diffusively buried into the bulk causing the surface energy to decrease after aging in air [25]. Additionally, WCA, OSEE and LIBS results all indicated that PDMS residues remained after ablation. Adhesive failure correlated better with the post-ablation OSEE $V_{th}$ signal (R = -0.67) than with the post-ablation WCA (R = 0.47). Also, less variability is observed in $V_{th}$ than in WCA as indicated by the error bars (one standard deviation) in figures 3 and 4.

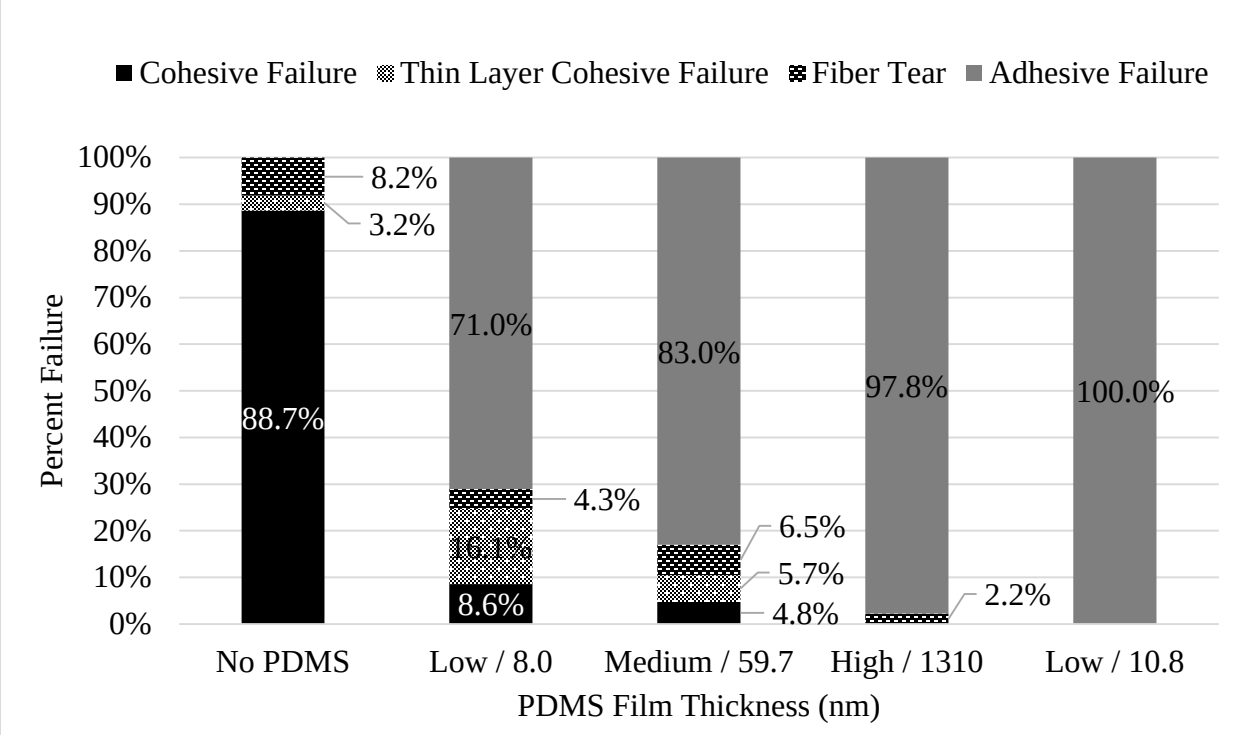


Figure 7: Average percent failure modes for varied PDMS film thickness. Except for the low/10.8 nm sample, all speciemens received laser ablation treatment after contamination.

### 3.4 Average Fracture Toughness

Fracture toughness ($G_{AVG}$) values are presented in Table 2 with average bondline thickness measurements. Although high $G_{AVG}$ values were observed in most samples, including those with contamination, these data were only obtained from steady crack growth occurring in regions of cohesive failure. In contaminated samples, unsteady crack growth occurred upon transition from cohesive failure to other lower-energy modes of failure, and no steady crack growth was observed for non-cohesive failure modes except for the highly contaminated sample. No $G_{AVG}$ was reported for the untreated sample because no steady crack growth was observed.

Table 2: Average fracture toughness ($G_{AVG}$) and bond measurement results.

| **Contamination level / treatment** | **Fracture Toughness ($kJ/m^2$)** | **Bondline Thickness (μm)** |
|---|---|---|
| No PDMS / laser | 2.88 ± 0.16 | 295 |
| Low / laser | 3.46 ± 0.09 | 276 |
| Medium / laser | 4.00 ± 0.26 | 286 |
| High / laser | 0.77 ± 0.23 | 280 |
| Low / none | NA | 304 |

## 4. CONCLUSIONS

Laser systems, which are inherently amenable to automation and closed-loop feedback control, may be necessary to achieve FAA certification of bonded primary structures. Laser surface preparation of epoxy matrix composites has been previously demonstrated to produce high performance adhesive bonds comparable to grit blasting. In this work, CFRP surfaces were contaminated with measured levels of PDMS, examined by WCA, OSEE, and LIBS and bonded for DCB testing. All forms of surface analysis correlated with the observed failure modes, which indicated that PDMS was partially removed during ablation. OSEE appeared to be more sensitive to PDMS contamination and yielded more repeatable data than WCA. Preliminary, μLIBS experiments also detected the presence of silicon on contaminated CFRP surfaces. Residual PDMS likely caused the poor bond performance after laser ablation of contaminated substrates. A two-fold mechanism was proposed for the redeposition and rearrangement of PDMS molecules to lower the surface energy after laser treatment. It was found that PDMS concentrations less than 0.8 $\mu g/cm^2$ (~8 nm thick) caused significant problems in adhesive bonding leading to predominantly adhesive failure in DCB specimens.

## 5. ACKNOWLEDGEMENTS

The authors thank John W. Hopkins for conducting the laser ablation surface treatment, Sean Britton and Hoa Luong for sample fabrication, Michael Oliver for specimen preparation, and Paul Bagby for photographic assistance. Thanks is also due to Louis Simmons for machining of composite specimens. Finally, thanks go to Tom Yost and Dan Perey for insightful discussions about OSEE technology.

## 6. REFERENCES

1. Russell, J., "Advanced composite cargo aircraft proves large structure practicality." *Composites World* 12/04/2009, 2010.
2. Bossi, R.; Piehl, M. J., "Bonding Primary Aircraft Structure: The Issues." *Manufacturing Engineering* **2011,** (March), 101-109.
3. Piehl, M. J.; Bossi, R. H.; Blohowiak, K. Y.; Dilligan, M. A.; Grace, W. B. "Efficient certification of bonded primary structure," Society for the Advancement of Materials and Process Engineering, Long Beach, Long Beach, 2013; pp 649-658.
4. Kruse, T.; Fuertes, T. A. S.; Koerwien, T.; Geistbeck, M. "Bonding of CFRP primary aerospace structures - boundary conditions for certification in relation with new design and technology developments," Society for the Advancement of Materials and Process Engineering, Seattle, WA, Seattle, WA, 2014.
5. Gardiner, G., "Building TRUST in bonded primary structures." *Composites World* 04/01/2015, 2015.
6. Oakley, B.; Bichon, B.; Clarkson, S.; Dillingham, G.; Hanson, B.; McFarland, J. M.; Palmer, M. J.; Popelar, C.; Weatherston, M. "TRUST - A novel approach to determine effects of archetype contaminant compounds on adhesion of structural composites," SAMPE 2015 Annual Meeting, Baltimore, Society for the Advancement of Material and Process Engineering: Baltimore, 2015.
7. Blohowiak, K. Y.; Voast, P. J. V.; Shelley, P. H.; Grob, J. W. "Nonchemical surface treatments using energetic systems for structual adheisve bonding," SAMPE 2010, Seattle, Society for the Advancement of Material and Process Engineering: Seattle, 2010.

8. Belcher, M. A. T.; Krieg, K. L.; Voast, P. J. V.; Blohowiak, K. Y. "Nonchemical surface treatments using atmostpheric plasma systems for structural adhesive bonding," SAMPE 2013 Annual Meeting, Long Beach, Society for the Advancement of Material and Process Engineering: Long Beach, 2013.
9. Hart-Smith, L. J.; Redmond, G.; Davis, M. J. "The curse of the nylon peel ply," 41st SAMPE International Symposium and Exhibition, Anaheim, CA, March 25-28; Anaheim, CA, 1994; pp 1-25.
10. Kanerva, M.; Saarela, O., "The peel ply surface treatment for adhesive bonding of composites: A review." *International Journal of Adhesion & Adhesives* **2013,** *43*, 60-69.
11. Fischer, F.; Kreling, S.; Dilger, K., "Surface structuring of CFRP by using modern excimer laser sources." *Physics Procedia* **2012,** *39*, 154-160.
12. Fischer, F.; Kreling, S.; Gaebler, F.; Delmdahl, R., "Using excimer lasers to clean CFRP prior to adhesvie bonding." *Reinforced Plastics* **2013,** *57* (5), 43-46.
13. Palmieri, F. L.; Watson, K. A.; Morales, G.; Williams, T.; Hicks, R.; Hicks, C. J.; Wohl, C. J.; Hopkins, J. W.; Connell, J. W. "Laser ablation surface preparation of Ti-6Al-4V for adhesive bonding," SAMPE 2012 Annual Meeting, Baltimore, MD, Society for the Advancement of Material and Process Engineering: Baltimore, MD, 2012.
14. Fischer, F.; Romoli, L.; Kling, R., "Laser-based repair of carbon fiber reinforced plastics." *CIRP Annals - Manufacturing Technology* **2010,** *59*, 203-206.
15. Palmieri, F. L.; Hopkins, J.; Wohl, C. J.; Lin, Y.; Connell, J. W.; Belcher, M. A. T.; Blohowiak, K. Y. "Laser surface preparation of epoxy composites for secondardy bonding: optimization of ablation depth," SAMPE 2015, Baltimore, MD, Society for the Advancement of Material and Process Engineering: Baltimore, MD, 2015.
16. Palmieri, F. L.; Belcher, M. A.; Wohl, C. J.; Blohowiak, K. Y.; Connell, J. W. "Laser ablation surface preparation of carbon fiber reinforced epoxy composites for adhesive bonding," SAMPE 2013 Annual Meeting, Long Beach, CA, Society for the Advancement of Material and Process Engineering: Long Beach, CA, 2013.
17. Vilmin, F.; Bazin, P.; Thibault-Starzyk, F.; Travert, A., "Speciation of adsorbates on surface of solids by infrared spectroscopy and chemometrics." *Analytica Chemica Acta* **2015,** *891*, 79-89.
18. Perey, D. "A portable surface contamination monitor based on the principle of optically stimulated electron emission (OSEE)." Hampton, 1996.
19. Ogieglo, W.; Werf, H. v. d.; Tempelman, K.; Wormeester, H.; Wessling, M.; Nijmeijer, A.; Benes, N. E., "n-Hexane induced swelling of thin PDMS films under non-equilibrium nanofiltration permeation conditions, resolved by spectroscopic ellipsometry." *Journal of Membrane Science* **2013,** *437*, 313-323.
20. Palik, E.; Gorachand, G., *Handbook of optical constants of solids.* Academic Press Inc.: 1997.
21. Herzinger, C. M.; Johs, B.; McGahan, W. A.; Woolam, J. A.; Paulson, W., "Ellipsometric determination of optical constants for silicon and thermally grown silicon dioxide via a mult-sample, multi-wavelength, multi-angle investigation." *Journal of Applied Physics* **1998,** *83* (6), 3323.
22. ASTM Standard D5528-13, 2013, "Standard Test Method for Mode I Interlaminar Fracture Toughness of Unidirectional Fiber-Reinforced Matrix Composites." ASTM International, West Conshohocken, PA, 2013, www.astm.org.
23. ASTM Standard D5573-99, D5573-ADJ 1999, "Standard Practice for Classifying Failure Modes in Fiber-Reinforced-Plastic (FRP) Joints." ASTM International, West Conshohocken, PA, 1999.

24. Tropmann, A.; Tanguy, L.; Koltay, P.; Zengerle, R.; Riegger, L., "Completely Superhydrophobic PDMS Surfaces for Microfluidics." *Langmuir* **2012,** *28* (22), 8292-8295.
25. Morra, M.; Occhiello, E.; Marola, R.; Garbassi, F.; Humphrey, P.; Johnson, D., "On the aging of oxygen plasma-treated polydimethylsiloxane surface." *Journal of Colloid and Interface Science* **1990,** *137*, 11-24.
26. Koizumi, H.; Lacmann, K.; Schmidt, W. F., "Light-induced electron emission from silicone oils." *J. Phys. D: Applied Physics* **1992,** *25* (1992), 857-861.
27. Kramida, A.; Ralchenko, Y.; Reader, J.; (2015), N. A. T., NIST Atomic Spectra Database (version 5.3). 12/15/2015 ed.; National Institute of Standards and Technology: Gaithersburg, MD, 2015.
28. Graubner, V.-M.; Jordan, R.; Nuyken, O.; Lippert, T.; Hauer, M.; Schnyder, B.; Wokum, A., "Incubation and ablation behavior of poly(dimethylsiloxane) for 266 nm irradiation." *Applied Surface Science* **2002,** *197-198*, 786-790.